

DOI: <https://doi.org/10.21123/bsj.2023.7955>

## Semi-Analytical Assessment of Magneto-Hydrodynamic Nano-Fluid Flow Jeffrey- Hamel Problem

*Saja I Abdulridah*\* 

*Abeer M Jasim* 

Department of Mathematics, College of Science, University of Basrah, Basrah, Iraq.

\*Corresponding author: [saja.issam2@gmail.com](mailto:saja.issam2@gmail.com)

E-mail address: [abeer.jassem@yahoo.com](mailto:abeer.jassem@yahoo.com)

Received 15/10/2022, Revised 4/2/2023, Accepted 5/2/2023, Published Online First 20/5/2023,  
Published 01/1/2024



This work is licensed under a [Creative Commons Attribution 4.0 International License](https://creativecommons.org/licenses/by/4.0/).

### Abstract:

In this paper, analyzing the non-dimensional Magnesium-hydrodynamics problem Using nanoparticles in Jeffrey-Hamel flow (JHF) has been studied. The fundamental equations for this issue are reduced to a three-order ordinary differential equation. The current project investigated the effect of the angles between the plates, Reynolds number, nanoparticles volume fraction parameter, and magnetic number on the velocity distribution by using analytical technique known as a perturbation iteration scheme (PIS). The effect of these parameters is similar in the converging and diverging channels except magnetic number that it is different in the divergent channel. Furthermore, the resulting solutions with good convergence and high accuracy for the different values of the physical parameters are in the form a power-series of the problem posed. The efficiency of this method is shown by comparison between for different cases between computed results with numerical solution and solutions by other methods.

**Keywords:** Analysis of Convergence, Magneto hydrodynamics, Nanofluid flow, Non-Parallel Plates, Nanoparticle.

### Introduction:

Fluid dynamics is a discipline of mathematics and physics concerned with the description and study of the movement of liquids and gases. The science of fluid dynamics is frequently separated into aerodynamics and hydrodynamics. Many physical elements influence fluid flow including fluid characteristics, flow speed, and the geometry of the solid surface, also there are three important fluid physical properties like viscosity, density, and compressibility. The study of flows between two parallel walls in converging/diverging channel is very important due to its engineering and industrial applications. Such applications include exchanging heat transfer of heat exchangers for milk flowing, cold drawing operation in polymer industry, extrusion of molten polymers through converging dies, pressure driven transport of particles through a symmetric converging/diverging channel and many others. Nano-fluids have novel properties that make them potentially useful in many applications in heat transfer, including microelectronics, fuel cells, pharmaceutical processes, and hybrid powered engines, domestic refrigerator, engine

cooling/vehicle thermal management, chiller, heat exchanger, in grinding, machining and in boiler flue gas temperature reduction. They exhibit enhanced thermal conductivity and the convective heat transfer coefficient compared to the base fluid. Knowledge of the rheological behavior of nanofluids is found to be critical in deciding their suitability for convective heat transfer applications<sup>1</sup>. Nano-fluids also have special acoustical properties and in ultrasonic fields display additional shear-wave reconversion of an incident compressional wave; the effect becomes more pronounced as concentration increases. Nano-fluids are fluids that include nanometer-sized particles called nanoparticles. The design of engineering for these fluids is considered suspensions nanoparticles in a base fluid. Metals, oxides, carbides, or carbon nanotubes are common nanoparticles utilized in nanofluids while water, ethylene glycol, and oil are examples of common base fluids. Nanofluids have unique properties that make them potentially useful in a wide range of heat transfer applications nanofluids also exhibit unique acoustical capabilities, displaying extra shear-wave

reconversion of an incident compressional wave in ultrasonic fields; the effect gets more apparent as concentration increases when compared to the base fluid. They have higher thermal conductivity and convective heat transfer coefficient. It has been discovered that understanding the rheological behavior of nanofluids is crucial in determining their appropriateness for convective heat transfer<sup>2</sup>. Nanofluid flow may be categorized into two types: compressible and incompressible. This categorization is based on the fluid density during the flow, which is constant for incompressible flow and changeable for compressible flow. Jeffrey<sup>3</sup> and Hamel<sup>4</sup> are among the most famous researchers of the last century whose studies focused on the flow of viscous, incompressible fluids through convergent and divergent channels. Furthermore, several approaches are investigated by many researchers for solving non-linear problems and the effects of Magnetohydrodynamic(MHD) for different fluids and geometries, such as<sup>5-8</sup>. In this paper, one of the most important approaches is employed for highly nonlinear problems, known as perturbation iteration scheme PIS(M,N)<sup>9-12</sup> where M is the number of correction terms in the perturbation expansion and N denotes the highest-order derivational term in the Taylor series, where M is always less than or equal to N. which is used to analyze an ordinary differential equations<sup>8</sup>. PIS is a type of analytical approach for discovering approximate-analytical solutions to nonlinear equations that cannot be solved exactly. It may be used to explain, forecast, and describe occurrences in systems induced by nonlinear processes<sup>13-16</sup>. This analytical approach has already been successfully applied to solve the problem of nanofluid flow, to find the analytic solutions for the velocity, and to study differential equations governing the MHD Jeffery-Hamel flow. In a base fluid water the impacts of nanoparticles (Al<sub>2</sub>O<sub>3</sub>, TiO<sub>2</sub>, Cu), Reynolds number, Hartmann number, angle open and volume fraction parameter on velocity profiles are graphically discussed. Consequently, the presented findings are compared in the literature with several analytical and numerical methods such as collocation method(CM), new analytical method (NAM), homotopy perturbation method (HPM<sup>24</sup>), spectral-homotopy analysis method (SHPM) and Range-Kutta of forth order (RK~4).

### Mathematical Formulation

The flow of an incompressible conductive viscous two dimensions fluid from a source or through at the intersection of non-parallel planar walls is presented. An electrically-driven boundary layer flow conductive viscous fluid containing

nanoparticles is taken into consideration. It is possible to describe the Jeffery-Hamel problem and the method of fluid flow on parallel walls geometrically as in Fig.1. The velocity is completely radial and solely dependent on r and  $\theta$  only<sup>14</sup>. In polar coordinates, the governing equations basic are defined mathematically as follows<sup>17-20</sup>:

$$\begin{aligned} \frac{\rho_{n.f}}{r} \frac{\partial(r\tilde{u})}{\partial r} &= 0, & 1 \\ \tilde{u} \frac{\partial \tilde{u}}{\partial r} + \frac{1}{\rho_{n.f}} \frac{\partial P}{\partial r} - \nu_{n.f} \left[ \frac{\partial^2 \tilde{u}}{\partial r^2} - \frac{1}{r} \frac{\partial \tilde{u}}{\partial r} - \frac{1}{r^2} \frac{\partial^2 \tilde{u}}{\partial \theta^2} + \frac{\tilde{u}}{r^2} \right] + \frac{\sigma \mu_0^2}{\rho_{n.f}} \tilde{u} &= 0, & 2 \\ \frac{1}{\rho_{n.f} r} \frac{\partial P}{\partial r} - \frac{2\nu_{n.f}}{r^2} \frac{\partial \tilde{u}}{\partial \theta} &= 0 & 3 \end{aligned}$$

Where  $\mu_0$  is electromagnetic induction,  $\tilde{u}$  is the radial velocity,  $\rho$  is the fluid density, p is the fluid pressure,  $\sigma$  is the conductivity of the nanofluid,  $\nu_{n.f}$  is the coefficient of kinematic viscosity. The fluid density, dynamic viscosity, kinematic viscosity, and  $\varphi$  as a solid volume fraction of nanofluid may be represented as follows:

- $\rho_{n.f} = (1 - \varphi)\rho_f + \varphi\rho_s,$
- $\mu_{n.f} = \frac{\mu_f}{(1-\varphi)^{2.5}},$  4
- $\nu_{n.f} = \frac{\mu_f}{\rho_{n.f}}.$

By integrating Eq. 1, with respect to r and setting the constant of integration  $\theta$  yield:

$$r\tilde{u}(r, \theta) = \omega(\theta), \quad 5$$

The derivation of Eqs. 2 and 3 with respect to r and  $\theta$  respectively, can be represent as

$$\frac{\tilde{u}(\partial^2 \tilde{u})}{\partial r \partial \theta} + \frac{\partial \tilde{u}}{\partial r} \frac{\partial \tilde{u}}{\partial \theta} = \nu_{n.f} \left[ \frac{\partial^3 \tilde{u}}{\partial r^2 \partial \theta} - \frac{3}{r} \frac{\partial^2 \tilde{u}}{\partial r \partial \theta} - \frac{1}{r^2} \frac{\partial^3 \tilde{u}}{\partial \theta^3} + \frac{3}{r^2} \frac{\partial \tilde{u}}{\partial \theta} \right] - \frac{\sigma \mu_0^2}{\rho_{n.f} r^2} \frac{\partial \tilde{u}}{\partial \theta}, \quad 6$$

The dimensionless variables with Eq. 5 can make the problem dimensionless

$$\omega(\xi) = \frac{\omega(\theta)}{\omega_{\max}}, \quad \omega(\xi) = \frac{r\tilde{u}(r, \theta)}{\omega_{\max}}, \quad \xi = \frac{\theta}{\lambda}, \quad \tilde{u}(r, \theta) = \frac{\omega_{\max}}{r} \omega(\xi), \quad 7$$

From Eq. 7, the required derivatives it will be:

$$\begin{aligned} \frac{\partial \tilde{u}}{\partial \theta} &= \frac{\omega_{\max}}{\lambda r} \frac{d\omega(\xi)}{d\xi}, & \frac{\partial^2 \tilde{u}}{\partial \theta^2} &= \\ \frac{\omega_{\max}}{\lambda^2 r} \frac{d^2 \omega(\xi)}{d\xi^2}, & \frac{\partial^3 \tilde{u}}{\partial \theta^3} &= \frac{\omega_{\max}}{\lambda^3 r} \frac{d^3 \omega(\xi)}{d\xi^3}, \\ \frac{\partial \tilde{u}}{\partial r} &= \frac{-\omega_{\max}}{r^2} \omega(\xi), & \frac{\partial^2 \tilde{u}}{\partial r^2} &= \\ \frac{2\omega_{\max}}{r^3} \omega(\xi), & \frac{\partial^2 \tilde{u}}{\partial r \partial \theta} &= \frac{-\omega_{\max}}{\lambda r^2} \frac{d\omega(\xi)}{d\xi}, \\ \frac{\partial^3 \tilde{u}}{\partial r^2 \partial \theta} &= \frac{2\omega_{\max}}{\lambda r^3} \frac{d\omega(\xi)}{d\xi}, & & 8 \end{aligned}$$

Substituting above partial derivative in Eq. 8, into Eq. 6, yield

$$\begin{aligned} \frac{-2\lambda^2 \omega_{\max}}{\nu_{n.f}} \omega(\xi) \frac{d\omega(\xi)}{d\xi} - \left[ 4\lambda^2 \frac{d\omega(\xi)}{d\xi} - \frac{d^3 \omega(\xi)}{d\xi^3} \right] + \frac{\sigma \mu_0^2 \lambda^2}{\rho_{n.f}} \nu_{n.f} \frac{d\omega(\xi)}{d\xi} &= 0, & 9 \end{aligned}$$

The simplification of Eq. 9, can appear as

$$\frac{d^3\omega(\xi)}{d\xi^3} - 2\lambda\tilde{R}_e \left[ (1-\varphi) + \varphi \frac{\rho_s}{\rho_f} \right] (1 - \varphi)^{2.5} \omega(\xi) \frac{d\omega(\xi)}{d\xi} + (4 - (1-\varphi)^{1.25} \tilde{H}_a) \lambda^2 \frac{d\omega(\xi)}{d\xi} = 0 \quad (10)$$

Subject to boundary conditions are

$$\omega(0) = 0, \quad \frac{d\omega(0)}{d\xi} = 0, \quad \omega(1) = 0, \quad (11)$$

where  $\tilde{R}_e = \frac{\omega_{max} \lambda}{\nu}$  is Reynolds number and  $\tilde{H}_a = \frac{\sigma \mu^2}{\rho \nu}$  is Hartmann number. In addition, can classified to two cases as:

- Divergence channel :  $\lambda > 0, \omega_{max} > 0,$
- Convergence channel :  $\lambda < 0, \omega_{max} < 0.$

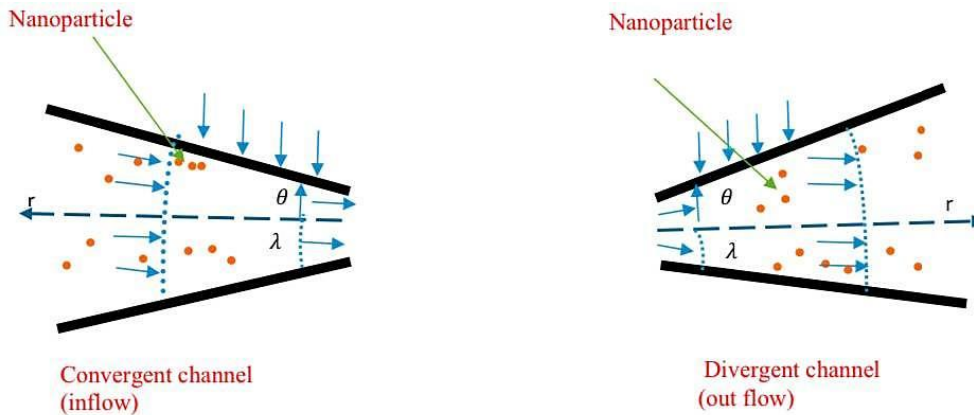


Figure 1. Geometry of JHF problem of convergent and divergent channel.

### Perturbation Iteration Scheme (PIS)

To illustrate the general of idea for PIS(1,1). Consider the nonlinear ordinary differential equation<sup>13-15</sup> as follows:

$$\mathcal{M} \left( \xi, \omega(\xi), \frac{d\omega(\xi)}{d\xi}, \frac{d^2\omega(\xi)}{d\xi^2}, \frac{d^3\omega(\xi)}{d\xi^3}, \dots, \frac{d^{(n-1)}\omega(\xi)}{d\xi^{(n-1)}}, \frac{d^{(n)}\xi(\xi)}{d\xi^{(n)}} \right) = 0, \quad (12)$$

where  $\omega$  is an unknown function and special dependent variable.  $\mathcal{M}$  is a function of  $\omega$  and its derivatives. The auxiliary perturbation parameter  $\delta$  can be added to Eq. 12, as indicated in the equation below

$$\mathcal{M} \left( \xi, \omega(\xi), \frac{d\omega(\xi)}{d\xi}, \frac{d^2\omega(\xi)}{d\xi^2}, \frac{d^3\omega(\xi)}{d\xi^3}, \dots, \frac{d^{(n-1)}\omega(\xi)}{d\xi^{(n-1)}}, \frac{d^{(n)}\omega(\xi)}{d\xi^{(n)}}, \delta \right) = 0, \quad (13)$$

Rewriting Eq. 13 with  $\delta$  is a small perturbation parameter as the following:

$$\mathcal{M} \left( \xi, \omega_{m+1}(\xi), \dot{\omega}_{m+1}(\xi), \ddot{\omega}_{m+1}(\xi), \dots, \omega_{m+1}^{(n-1)}(\xi), \omega_{m+1}^{(n)}(\xi), \delta \right) = 0, \quad (14)$$

where represents  $m$  the  $m^{th}$  iteration with define perturbation expansions with correction term as follow:

$$\omega_1 = \omega_0 + \delta(\omega_c)_0,$$

$$\omega_2 = \omega_1 + \delta(\omega_c)_1,$$

$$\omega_3 = \omega_2 + \delta(\omega_c)_2,$$

$$\vdots$$

$$\omega_{m+1} = \omega_m + \delta(\omega_c)_m, \quad (15)$$

where  $\omega_c$  is the correction term in the perturbation expansion and substituting Eq. 15 in Eq. 14, get:

$$\mathcal{M}(\xi, \omega_m(\xi) + \delta(\omega_c)_m, \dot{\omega}_m(\xi) + \delta(\dot{\omega}_c)_m, \ddot{\omega}_m(\xi) + \delta(\ddot{\omega}_c)_m, \dots, \omega_m^{(n-1)}(\xi) + \delta(\omega_c)_m^{(n-1)}, \omega_m^{(n)}(\xi) + \delta(\omega_c)_m^{(n)}, \delta) = 0, \quad (16)$$

now, using the Taylor series expansion for the first order derivative in the vicinity of  $\delta = 0$ , which gives:

$$\mathcal{M} \left( \xi, \omega_m(\xi), \frac{d\omega_m(\xi)}{d\xi}, \frac{d^2\omega_m(\xi)}{d\xi^2}, \dots, \frac{d^{(n-1)}\omega_m(\xi)}{d\xi^{(n-1)}}, \frac{d^{(n)}\omega_m(\xi)}{d\xi^{(n)}}, 0 \right) + \frac{d\mathcal{M}}{d\omega_m} \cdot (\omega_c)_m \Big|_{\delta=0} +$$

$$\delta \frac{d\mathcal{M}}{d\dot{\omega}_m} \cdot (\dot{\omega}_c)_m \Big|_{\delta=0} + \dots + \delta \frac{d\mathcal{M}}{d\omega_m^{(n-1)}} \cdot (\omega_c)_m^{(n-1)} \Big|_{\delta=0} + \delta \frac{d\mathcal{M}}{d\omega_m^{(n)}} \cdot (\omega_c)_m^{(n)} \Big|_{\delta=0} = 0, \quad (17)$$

Arrange Eq. 17 to get:

$$\begin{aligned}
 (\omega_c)_m^{(n)} &= \frac{-\mathcal{M}}{\delta \cdot \frac{d\mathcal{M}}{d\omega_m^{(n)}}} - \frac{\frac{d\mathcal{M}}{d\omega_m}}{\frac{d\mathcal{M}}{d\omega_m^{(n)}}} \cdot (\omega_c)_m - \frac{\frac{d\mathcal{M}}{d\dot{\omega}_m}}{\frac{d\mathcal{M}}{d\omega_m^{(n)}}} \cdot (\dot{\omega}_c)_m - \\
 &\dots - \frac{\frac{d\mathcal{M}}{d\omega_m^{(n-1)}}}{\frac{d\mathcal{M}}{d\omega_m^{(n)}}} \cdot (\omega_c)_m^{(n-1)} - \frac{\frac{d\mathcal{M}}{d\delta}}{\frac{d\mathcal{M}}{d\omega_m^{(n)}}} \cdot \delta
 \end{aligned} \quad 18$$

Note that all derivatives in Eq.18 are calculated at  $\delta = 0$ , the solution in Eq. 11 is an ordinary differential equation (ODE). The boundary condition and initial condition are used to solve this ordinary differential equation, yielding  $(\omega_c)_m(\xi)$ . In Eq.16, the value of  $(\omega_c)_m(\xi)$  is replaced to obtain on  $(\omega)_{m+1}(\xi)$ . Which it is the approximate analytical answer, in the form of a power series, that is required.

$$\begin{aligned}
 (\omega_c)_0^{(n)} &= \frac{-\mathcal{M}}{\delta \cdot \frac{d\mathcal{M}}{d\omega_0^{(n)}}} - \frac{\frac{d\mathcal{M}}{d\omega_0}}{\frac{d\mathcal{M}}{d\omega_0^{(n)}}} \cdot (\omega_c)_0 - \frac{\frac{d\mathcal{M}}{d\dot{\omega}_0}}{\frac{d\mathcal{M}}{d\omega_0^{(n)}}} \cdot (\dot{\omega}_c)_0 - \\
 &\dots - \frac{\frac{d\mathcal{M}}{d\omega_0^{(n-1)}}}{\frac{d\mathcal{M}}{d\omega_0^{(n)}}} \cdot (\omega_c)_0^{(n-1)} - \frac{\frac{d\mathcal{M}}{d\delta}}{\frac{d\mathcal{M}}{d\omega_0^{(n)}}} \cdot \delta
 \end{aligned} \quad 19$$

Thus, express the analytical approximate solutions in the following way, firstly define

$$\omega_0 = \mathbb{C}_0, \quad (\omega_c)_m = \mathbb{C}_{m+1},$$

and the remaining solutions can be developed in subsequent iterations

$$\omega_0 = \mathbb{C}_0,$$

$$\omega_1 = \omega_0 + (\omega_c)_0 = \mathbb{C}_0 + \mathbb{C}_1,$$

$$\omega_2 = \omega_1 + (\omega_c)_1 = \mathbb{C}_0 + \mathbb{C}_1 + \mathbb{C}_2,$$

:

$$\omega_{m+1} = \omega_m + (\omega_c)_m = \mathbb{C}_0 + \mathbb{C}_1 + \mathbb{C}_2 + \dots +$$

$$\mathbb{C}_{m+1} = \sum_{i=0}^{m+1} \mathbb{C}_i. \quad 20$$

As a result, the value of  $(\omega_c)_m$  is substituted in Eq. 16 to yield  $\omega_{m+1}(\xi)$  which takes the form of a power series. The analytical approximate solution to Eq. 12, is as follows:

$$\omega = \lim_{m \rightarrow \infty} \omega_{m+1} = \sum_{i=0}^{\infty} \mathbb{C}_i.$$

### The Application of PIS for Jeffery-Hamel Nano-fluid Flow

The steps of PIS (1,1) to the Jeffery-Hamel Nanofluid Flow problem in order to find an analytical solution, can be illustrated as follows;

$$\begin{aligned}
 \frac{d^3\omega(\xi)}{d\xi^3} - 2\lambda\tilde{R}_e \left[ (1-\varphi) \right. \\
 \left. + \varphi \frac{\rho_s}{\rho_f} \right] (1-\varphi)^{2.5} \omega(\xi) \frac{d\omega(\xi)}{d\xi} + \\
 (4 - (1-\varphi)^{1.25} \tilde{H}_a) \lambda^2 \frac{d\omega(\xi)}{d\xi} = 0,
 \end{aligned} \quad 21$$

the JHF of auxiliary perturbation parameter is

$$\begin{aligned}
 \mathcal{M} \left( \omega(\xi), \frac{d\omega(\xi)}{d\xi}, \frac{d^3\omega(\xi)}{d\xi^3}, \delta \right) &= \frac{d^3\omega(\xi)}{d\xi^3} + 2\delta\lambda\tilde{R}_e((1-\varphi) \\
 &+ \frac{\rho_s}{\rho_f} \varphi) (1-\varphi)^{2.5} \omega(\xi) \frac{d\omega(\xi)}{d\xi} \\
 &+ \delta(4 - (1-\varphi)^{1.25} \tilde{H}_a) \lambda^2 \frac{d\omega(\xi)}{d\xi}.
 \end{aligned} \quad 22$$

The general equation of Perturbation expansion is  $\omega_{n+1} = \omega_n + \delta(\omega_c)_n$ , substituting Eq. 22 and Eq. 23, and expanding using the Taylor series of first order derivatives about ( $\delta = 0$ ), give

$$\mathcal{M}(\omega_n, \dot{\omega}_n, \ddot{\omega}_n, 0) + \delta[\mathcal{M}_{\omega_n}(\omega_c)_n + \mathcal{M}_{\dot{\omega}_n}(\omega_c)_n + \mathcal{M}_{\ddot{\omega}_n}(\omega_c)_n + \mathcal{M}_{\delta}] = 0, \quad 24$$

from Eq. 16, the following of the partial derivatives:

$$\mathcal{M}_{\delta} = 2\lambda\tilde{R}_e((1-\varphi) + \frac{\rho_s}{\rho_f} \varphi)(1-\varphi)^{2.5} \omega_n \dot{\omega}_n -$$

$$(4 - (1-\varphi)^{1.25} \tilde{H}_a) \lambda^2 \dot{\omega}_n,$$

$$\mathcal{M}_{\omega_n} = 2\delta\lambda\tilde{R}_e((1-\varphi) + \frac{\rho_s}{\rho_f} \varphi)(1-\varphi)^{2.5} \dot{\omega}_n,$$

$$\mathcal{M}_{\dot{\omega}_n} = 2\delta\lambda\tilde{R}_e((1-\varphi) + \frac{\rho_s}{\rho_f} \varphi)(1-\varphi)^{2.5} \omega_n,$$

$$\mathcal{M}(\omega_n, \dot{\omega}_n, \ddot{\omega}_n, 0) = \ddot{\omega}_n,$$

$$\mathcal{M}_{\ddot{\omega}_n} = 1. \quad 25$$

By calculating all partial derivatives at  $\delta = 0$  and substituting the results into Eq. 24, led to

$$\begin{aligned}
 (\ddot{\omega}_c)_n &= -\frac{1}{\delta} \ddot{\omega}_n - 2\lambda\tilde{R}_e((1-\varphi) + \frac{\rho_s}{\rho_f} \varphi) \\
 &(1-\varphi)^{2.5} \omega_n \dot{\omega}_n - (4 - (1-\varphi)^{1.25} \tilde{H}_a) \lambda^2 \dot{\omega}_n,
 \end{aligned} \quad 26$$

the initial condition of the Eq. 21, become

$$\omega_0(\xi) = \mathbb{Z}_0 + \mathbb{Z}_1 \xi + \mathbb{Z}_2 \frac{\xi^2}{2!}, \quad 27$$

where,

$$\omega(0) = \mathbb{Z}_0, \quad \frac{d\omega(0)}{d\xi} = \mathbb{Z}_1, \quad \frac{d^2\omega(0)}{d\xi^2} = \mathbb{Z}_2.$$

From boundary conditions Eq. 11:

$$\omega_0(\xi) = 1 + \mathbb{Z}_2 \frac{\xi^2}{2}. \quad 28$$

Note that having a preliminary condition for solving the equation that involves the unknown  $\mathbb{Z}_2$ , can calculate the value of  $\mathbb{Z}_2$  using the resulted solution of JHF problem at a value of  $\xi = 1$ . The analytical obtained solutions can be written as follows:

$$\begin{aligned}
 \omega_1(\xi) &= 1 + \frac{\mathbb{Z}_2}{2} \xi^2 - \left[ \frac{1}{12} \lambda\tilde{R}_e((1-\varphi) \right. \\
 &+ \frac{\rho_s}{\rho_f} \varphi)(1-\varphi)^{2.5} \\
 &- \frac{1}{24} ((1-\varphi)^{1.25} \tilde{H}_a - 4\lambda^2) \mathbb{Z}_2 \xi^4 \\
 &- \left. \frac{1}{120} ((1-\varphi) + \frac{\rho_s}{\rho_f} \varphi)(1-\varphi)^{2.5} \lambda\tilde{R}_e \mathbb{Z}_2^2 \right] \xi^6,
 \end{aligned} \quad 29$$

$$\begin{aligned}
 \omega_2(\xi) &= 1 + \frac{\mathbb{Z}_2}{2} \xi^2 + \left[ -\frac{1}{12} ((1-\varphi) + \frac{\rho_s}{\rho_f} \varphi)(1-\varphi)^{2.5} \lambda\tilde{R}_e \mathbb{Z}_2 \right. \\
 &+ \frac{1}{24} (1-\varphi)^{1.25} \tilde{H}_a \mathbb{Z}_2 - \\
 &\left. \frac{1}{6} \lambda^2 \mathbb{Z}_2^2 \right] \xi^4 - \frac{1}{120} ((1-\varphi) + \frac{\rho_s}{\rho_f} \varphi)(1-\varphi)^{2.5} \lambda\tilde{R}_e \mathbb{Z}_2^3 \xi^6,
 \end{aligned}$$

$$\begin{aligned}
 & \varphi)^{2.5} \lambda \tilde{R}_e Z_2^2 + \frac{1}{180} ((1 - \varphi) + \frac{\rho_s}{\rho_f} \varphi)^2 (1 - \varphi)^5 \\
 & \quad \lambda^2 \tilde{R}_e^2 Z_2 + \frac{1}{45} ((1 - \varphi) + \frac{\rho_s}{\rho_f} \varphi) (1 - \\
 & \varphi)^{2.5} \lambda^3 \tilde{R}_e Z_2 - \frac{1}{90} (1 - \varphi)^{1.25} \lambda^2 \tilde{H}_a Z_2 + \\
 & \quad \lambda^2 \tilde{R}_e^2 Z_2^2 + \frac{1}{280} (1 - \varphi) + \frac{\rho_s}{\rho_f} \varphi) (1 - \\
 & \varphi)^{2.5} \lambda^3 \tilde{R}_e Z_2^2 - \frac{1}{1120} (1 - \varphi) + \frac{\rho_s}{\rho_f} \varphi) (1 - \varphi)^{3.75} \\
 & \quad \lambda \tilde{R}_e \tilde{H}_a Z_2^2] \xi^8 + (\frac{1}{10800} ((1 - \varphi) + \\
 & \frac{\rho_s}{\rho_f} \varphi)^2 \lambda^2 \tilde{R}_e^2 Z_2^3 - \frac{1}{12960} ((1 - \varphi) + \frac{\rho_s}{\rho_f} \varphi)^3 (1 - \varphi)^{7.5} \\
 & \quad \lambda^3 \tilde{R}_e^3 Z_2^3 - \frac{1}{3240} ((1 - \varphi) + \frac{\rho_s}{\rho_f} \varphi)^3 (1 - \\
 & \varphi)^{7.5} \lambda^4 \tilde{R}_e^2 C_2^2 - \frac{1}{3240} (1 - \varphi)^{1.25} \lambda^3 \tilde{R}_e \tilde{H}_a Z_2^2 + \\
 & \quad \frac{1}{12960} ((1 - \varphi) + \frac{\rho_s}{\rho_f} \varphi)^2 (1 - \\
 & \varphi)^{6.25} \lambda^2 \tilde{R}_e^2 \tilde{H}_a Z_2^2 - \frac{1}{51840} (1 - \varphi) + \frac{\rho_s}{\rho_f} \varphi) \\
 & \quad \tilde{R}_e \tilde{H}_a Z_2^2 + \frac{1}{6480} (1 - \varphi) + \frac{\rho_s}{\rho_f} \varphi) (1 - \\
 & \varphi)^{3.75} \lambda^3 \tilde{R}_e \tilde{H}_a Z_2^2] \xi^{10} + [-\frac{1}{95040} ((1 - \varphi) + \\
 & \frac{\rho_s}{\rho_f} \varphi)^3 (1 - \varphi)^{7.5} \\
 & \quad \lambda^3 \tilde{R}_e^3 Z_2^3 - \frac{1}{47520} ((1 - \varphi) + \frac{\rho_s}{\rho_f} \varphi)^2 (1 - \\
 & \varphi)^5 \lambda^4 \tilde{R}_e^2 Z_2^3 + \frac{1}{190080} ((1 - \varphi) + \frac{\rho_s}{\rho_f} \varphi)^2 \\
 & \quad (1 - \varphi)^{7.5} \lambda^2 \tilde{R}_e^2 \tilde{H}_a Z_2^3] \xi^{12} \quad 30 \\
 & :
 \end{aligned}$$

## Results and Discussion

Discussions of various flow parameters (Hartmann, nanofluid volume fraction, and Reynold numbers) on the velocity profile  $\omega(\xi)$  are included in this section. Firstly, Table 1 shows the physical material in state of density, thermal conductivity and specific heat capacity for (water  $Al_2O_3$ ,  $TiO_2$  and  $Cu$ ). The convergence of values  $Z_2$  is clearly shown in Tables 2 and 3. The PIS findings are presented in Tables 4-8 and compared to the numerical, collocation technique solutions and other methods. The results are totally compatible, as shown in the tables, also, when observing Tables 5, 7, and 8, when making the error between the method we are working on and the numerical methods in the literature, we note that the PIS is the best in terms of solutions and excellent compatibility with the numerical methods, so this gives us preference to take it and work with it in the subsequent fields. This precision instills in us a high level of trust in the validity of the problem and demonstrates a high level of engineering precision agreement. This inquiry is finished by illustrating the impacts of a few key factors in order to determine how these variables affect the fluid. Figs. 2-4, illustrate the impact of various active parameter settings.

**Material  $Al_2O_3$ .** The impact of the Hartmann number on the velocity profiles of divergent and convergent channels is seen in Fig. 2a. The results

reveal that raising the Hartmann number raises the velocity profiles of both convergent and divergent channels. As the Hartmann number rises, it becomes clear that there is no backflow in both channels. Figure 2b illustrates that in divergent channels, fluid velocity falls with Reynolds numbers, whereas in convergent channels, fluid velocity increases with Reynolds numbers. According to Fig. 2c, the fluid velocity tends to decrease as the nanofluid volume fraction increases in divergent channels but increases in convergent channels.

**Material  $TiO_2$ .** Figure 3a shows the result of raising the Hartmann number on the velocity profiles of divergent and convergent channels. The velocity profiles of convergent and divergent channels are reduced as a result. There is no backflow in both channels when the Hartmann number increased. In both divergent and convergent channels, the fluid velocity decreases with increasing Reynolds numbers, as seen in Fig. 3b. The fluid velocity reduces with increasing nanofluid volume fraction in divergent channels but increases with nanofluid volume fraction in convergent channels, as shown in Fig. 3c.

**Material  $Cu$ .** Figure 4a, illustrates the impact of the Hartmann number on the velocity profiles of divergent and convergent channels. It's worth noting that when the Hartmann number rises, the velocity profiles of convergent and divergent channels decrease. Furthermore, raising the Hartmann number in both channels results in no backflow, which is plainly visible. Figure 4b, shows that in divergent channels, the fluid velocity falls as the Reynolds number increases, whereas in convergent channels, the fluid velocity increases. Fluid velocity decreases with increasing nanofluid volume fraction in divergent channels, but rises in convergent channels, as seen in Fig. 4c.

The effect of changing the angle yielding to increases the profile of velocity as clear in Fig. 2d, 3d and 4d, for  $Al_2O_3$ ,  $TiO_2$ , and  $Cu$  respectively. In the convergent channel, the increase is evident in the effect of the angle on the velocity profile curves, but the opposite can be seen in the divergent channel. The rise of the Reynolds number has an effect on the convergence of the solutions as shown in the behavior of the velocity in the figures in the divergent channel only, notice the deviated of the curve at  $\lambda = 20^\circ$  in  $\xi = 0.65$ . It can also be noted that there is no effect when an increase in the Reynolds number of the converging channel in increasing the velocity curves in all cases as shown in Fig. 2d, 3d and 4d.

Physically, the impact of the Reynolds number on the velocity distribution is due to higher viscosity at the border, which causes fluid motion

resistance and hence an increase in the momentum boundary layer. The influence of nanofluid volume fraction on velocity is shown, with a steady drop in velocity profile as the nanofluid volume fraction rises. When  $\varphi = 0$  in this plot, the fluid is transported down the channel with no nanofluid volume percentage. Given the significant energy exchange rate when fluid molecules flow through the nonparallel channel, nanofluid volume fraction has an influence on the fluid and lowers the thickness of the momentum barrier layer. The influence of channel opening angles on the divergent- convergent plate. To prevent fluid backflow, relatively broad open channel angles are used. Backflow is not a problem in the converging channel, but it can happen

in the diverging channel. Backflow is prevented by a high Reynolds number in the presence of a strong magnetic field strength. As shown, increasing the channel angle quantitatively results in a considerable drop in the velocity profile. The magnetic field effects flow, as seen by the magnetic field intensity and the reduction in fluid flow via the nonparallel channel. As can be seen in the plot, absolute velocity decreases. This may be explained physically by the existence of resistive forces at the channel's border owing to an increase in boundary layer thickness, which causes a retarding effect on the velocity field. Now, some tables and figures will be reviewed that changed values of  $\tilde{R}_e$ ,  $\tilde{H}_a$  and  $\varphi$  as follow:

**Table 1. Properties of Nanofluid and Nanoparticles**

Item	$\rho(\text{kg/m}^3)$	CP(J/kgK)	k(W/mK)
Al <sub>2</sub> O <sub>3</sub>	3970	765	40
TiO <sub>2</sub>	4250	686.2	8.9538
Cu	8933	385	401
fluid phase(water)	997.1	4179	0.613

**Table 2. The convergence of the fixed values when  $\varphi = 0.001$**

Order	$\tilde{R}_e = 30, \tilde{H}_a = 700$		$\tilde{R}_e = 30, \tilde{H}_a = 600$		$\tilde{R}_e = 20, \tilde{H}_a = 200$	
	$\lambda = 2^\circ$		$\lambda = 3^\circ$		$\lambda = 5^\circ$	
	$\mathbb{Z}_2$		$\mathbb{Z}_2$		$\mathbb{Z}_2$	
Class 1	-2.166866549	-2.103282989	-2.229756176			
Class 2	-2.165203558	-2.105260852	-2.228845350			
Class 3	-2.165221284	-2.105264580	-2.228865090			
Class 4	-2.165221197	-2.105264601	-2.228865106			
Class 5	-2.165221197	-2.105264601	-2.228865106			

**Table 3. The convergence of the fixed values when  $\phi = 0.001$**

Order	$\tilde{R}_e = 30, \tilde{H}_a = 700$		$\tilde{R}_e = 30, \tilde{H}_a = 600$		$\tilde{R}_e = 20, \tilde{H}_a = 200$	
	$\lambda = -2^\circ$		$\lambda = -3^\circ$		$\lambda = -5^\circ$	
	$\mathbb{Z}_2$		$\mathbb{Z}_2$		$\mathbb{Z}_2$	
Class 1	-1.657407	-1.445386	-1.45574			
Class 2	-1.638453	-1.393417	-1.40676			
Class 3	-1.637772	-1.389896	-1.40360			
Class 4	-1.637756	-1.389740	-1.40347			
Class 5	-1.637756	-1.389740	-1.40347			

**Table 4. The profile of  $\omega(\xi)$  for  $TiO_2$**

$\xi$	$\tilde{R}_e = 50, \tilde{H}_a = 0, \varphi = 0, \lambda = 5^\circ$	$\tilde{R}_e = 10, \tilde{H}_a = 750, \varphi = 0.05, \lambda = -5^\circ$	$\tilde{R}_e = 30, \tilde{H}_a = 600, \varphi = 0.02, \lambda = 5^\circ$
0.00	1.0000000000	1.0000000000	1.0000000000
0.05	0.9955850163	0.9985407480	0.9975322023
0.10	0.9824360737	0.9941370402	0.9901341560
0.20	0.9312441318	0.9761297024	0.9606182178
0.30	0.8506474508	0.9446966965	0.9116655867
0.40	0.7468472460	0.8976157250	0.8435286562
0.50	0.6270205939	0.8315921452	0.7563476197
0.60	0.4983152995	0.7420743222	0.6499430042
0.70	0.3670452811	0.6230187448	0.5235488252
0.75	0.3020636550	0.5500506880	0.4523740775
0.80	0.2381888793	0.4666155463	0.3754720632
0.85	0.1758023208	0.3714135480	0.2924130170
0.90	0.1151907682	0.2629998131	0.2026445163
0.95	0.05655169989	0.1397785248	0.1054664173
1.00	0.0000000000	0.0000000000	0.0000000000

**Table 5. The profile of  $\omega(\xi)$  for Cu**

$\xi$	$\tilde{R}_e = 30, \tilde{H}_a = 600, \lambda = 5^\circ, \varphi = 0.02$				
	PIS	NAM <sup>17</sup>	RK~4	Residual error (PIS,RK~4)	Residual error (NAM,RK~4)
0.00	1.000000000	1.000000000	1.000000000	0.000000000	0.000000000
0.10	0.9898438613	0.989837623	0.989843868	0.000000006	0.000006245
0.20	0.9595061889	0.959481313	0.959506219	0.000000030	0.000024906
0.30	0.9093422847	0.909286554	0.909342349	0.000000064	0.000055795
0.40	0.8398237017	0.839725036	0.839823811	0.000000109	0.000098775
0.50	0.7513647610	0.751210824	0.751364924	0.000000163	0.000154100
0.60	0.6440902848	0.643867387	0.644090515	0.000000231	0.000223128
0.70	0.5175457664	0.517236610	0.517546090	0.000000324	0.000309480
0.80	0.3703390664	0.369919206	0.370339540	0.000000474	0.000420340
0.90	0.1996813580	0.199115412	0.199682092	0.000000734	0.000566680
1.00	0.000000000	0.000000000	0.000000000	0.000000000	0.000000000

**Table 6. The profile of  $\omega(\xi)$  for Cu when  $\tilde{R}_e = 50, \tilde{H}_a = 0, \lambda = 5^\circ, \varphi = 0$ .**

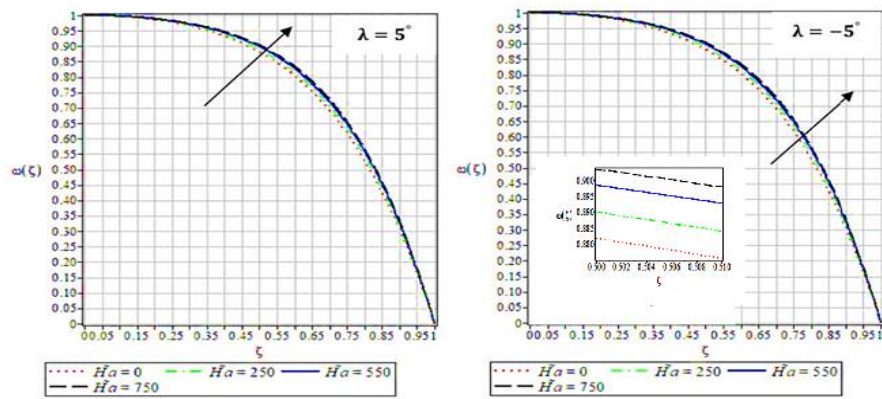
$\xi$	PIS	Reference <sup>17</sup>	HPM <sup>19</sup>	SHPM <sup>19</sup>	Reference <sup>21</sup>	Reference <sup>22</sup>	RK~4
0.00	1.000000	1.000000	1.000000	1.000000	1.000000	1.000000	1.000000
0.25	0.894269	0.894649	0.894960	0.894242	0.894242	0.894243	0.894269
0.50	0.627020	0.628312	0.627220	0.626948	0.626948	0.626953	0.627022
0.75	0.302063	0.303771	0.302001	0.301990	0.301991	0.301998	0.302065
1.00	0.000000	0.000000	0.000000	0.000000	0.000000	0.000000	0.000000

**Table 7. The profile of  $\omega(\xi)$  for Cu**

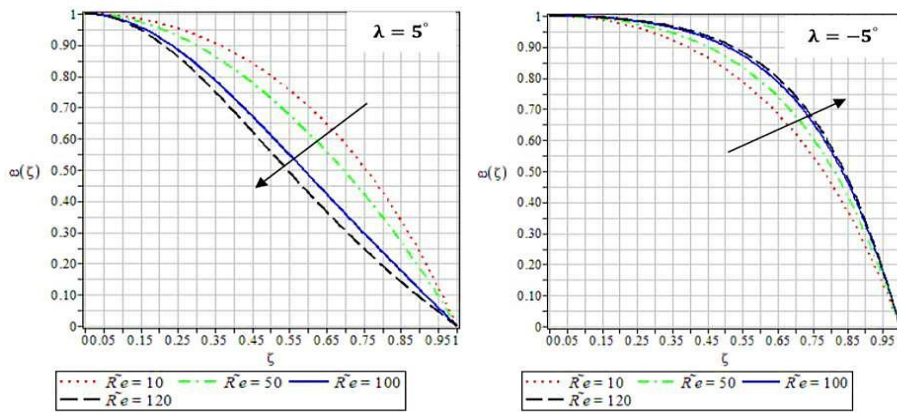
$\xi$	$\tilde{R}_e = 10, \tilde{H}_a = 750, \lambda = -5^\circ, \varphi = 0.05$				
	PIS	NAM <sup>17</sup>	CM <sup>23</sup>	Residual error (PIS,CM)	Residual error (NAM,CM)
0.00	1.000000000	1.000000000	1.000000000	0.000000000	0.000000000
0.10	0.9942690739	0.994237767	0.994278317	0.0000092431	0.000040550
0.20	0.9766464658	0.976518907	0.976670165	0.0000236992	0.000151258
0.30	0.9458150013	0.945519431	0.945855446	0.0000404447	0.000336015
0.40	0.8994867526	0.898941811	0.899546175	0.0000594224	0.000604364
0.50	0.8342633380	0.833382035	0.834341990	0.0000786520	0.000959955
0.60	0.7454407460	0.744151771	0.745536091	0.0000953450	0.001378381
0.65	0.6902932180	0.688792461	0.690394661	0.0001014430	0.001602200
0.70	0.6267640959	0.625067799	0.626869073	0.0001049771	0.001801274
0.75	0.5537831903	0.551934739	0.553888111	0.0001049207	0.001953372
0.80	0.4701479955	0.468230004	0.470248161	0.0001001655	0.002018157
0.85	0.3745158259	0.372665147	0.374605389	0.0000895631	0.001940242
0.90	0.2653976864	0.263823428	0.265469361	0.0000716746	0.001645933
0.95	0.1411549204	0.140159099	0.141198775	0.0000438546	0.001039676
1.00	0.000000000	0.000000000	0.000000000	0.000000000	0.000000000

**Table 8. The profile of  $\omega(\xi)$  for  $Al_2O_2$**

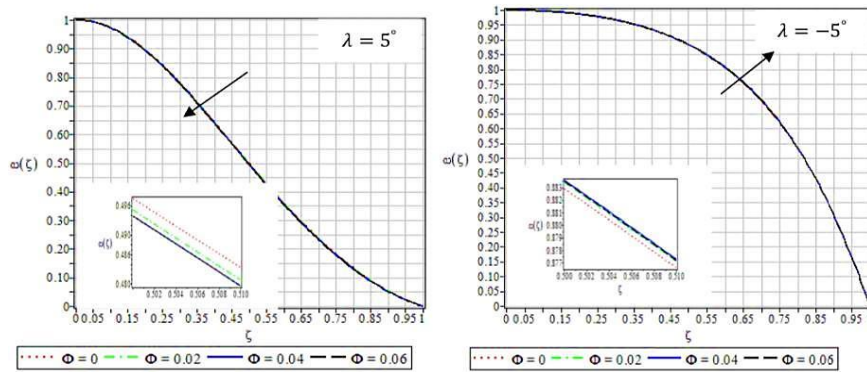
$\xi$	$\tilde{R}_e = 10, \tilde{H}_a = 0, \lambda = -3^\circ, \varphi = 0.01$				
	Present solution	Reference <sup>17</sup>	Numerical method <sup>22</sup>	Residual error (PIS,NM)	Residual error (Reference <sup>17</sup> ,NM)
0.10	0.9892746750	0.989274758	0.989274758	0.000000083	0.000000000
0.15	0.9758945272	0.975894713	0.975894718	0.000000190	0.000000005
0.20	0.9572113072	0.957211638	0.957211647	0.000000339	0.000000009
0.25	0.9332729078	0.933273423	0.933273437	0.000000529	0.000000014
0.30	0.9041393503	0.904140089	0.904140111	0.000000760	0.000000022
0.35	0.8698816537	0.869882653	0.869882686	0.000001032	0.000000033
0.40	0.8305804780	0.830581769	0.830581821	0.000001343	0.000000052
0.45	0.7863245615	0.786326170	0.786326255	0.000001693	0.000000085
0.50	0.7372089770	0.737210915	0.737211060	0.000002083	0.000000145
0.55	0.6833332169	0.683335479	0.683335727	0.000002510	0.000000248
0.60	0.6247991314	0.624801686	0.624802106	0.000002974	0.000000042
0.65	0.5617087387	0.561711523	0.561712214	0.000003475	0.000000691
0.70	0.4941619214	0.494164834	0.494165934	0.000004012	0.000001100
0.75	0.4222540321	0.422256931	0.422258619	0.000004586	0.000001688
0.80	0.3460734116	0.346076117	0.346078608	0.000005196	0.000002491
0.85	0.2656988314	0.265701137	0.265704674	0.000005842	0.000003537
0.90	0.1811968752	0.181198571	0.181203403	0.000006527	0.000004832
0.95	0.0926192463	0.092620147	0.092626497	0.000007250	0.000006350
1.00	0.000000000	0.000000000	0.000008010	0.000000000	0.000000000



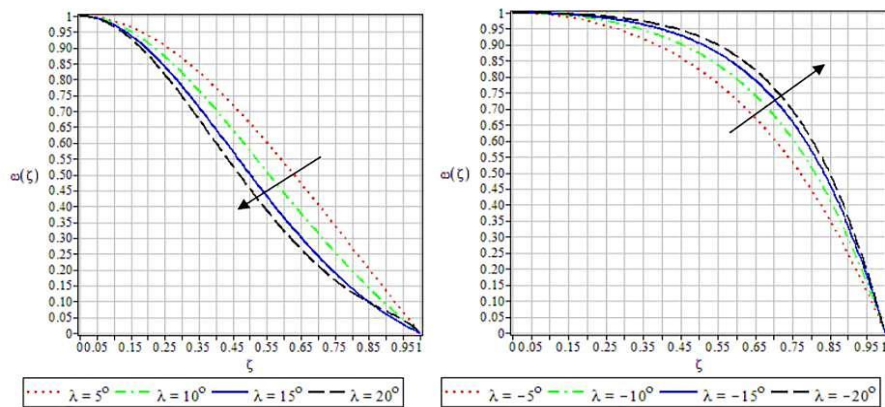
(a)  $\tilde{H}_a$  varied for  $\tilde{R}_e = 100, \varphi = 0.05$



(b)  $\tilde{R}_e$  varied for  $\tilde{H}_a = 50, \varphi = 0.05$

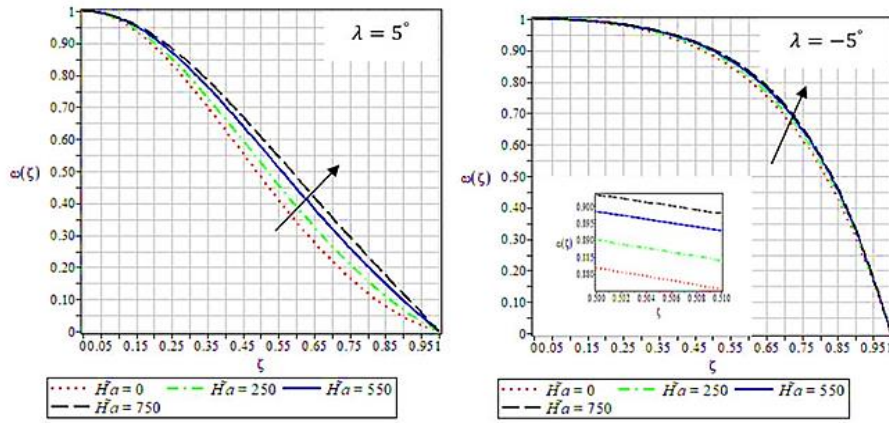


(c)  $\varphi$  varied for  $\tilde{H}_a = 50, \tilde{R}_e = 100$

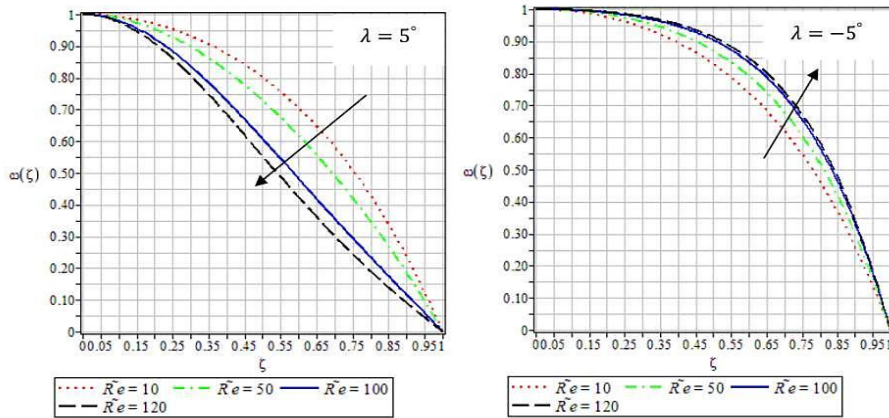


(d)  $\lambda$  varied for  $\tilde{H}_a = 50, \tilde{R}_e = 40, \varphi = 0.05$

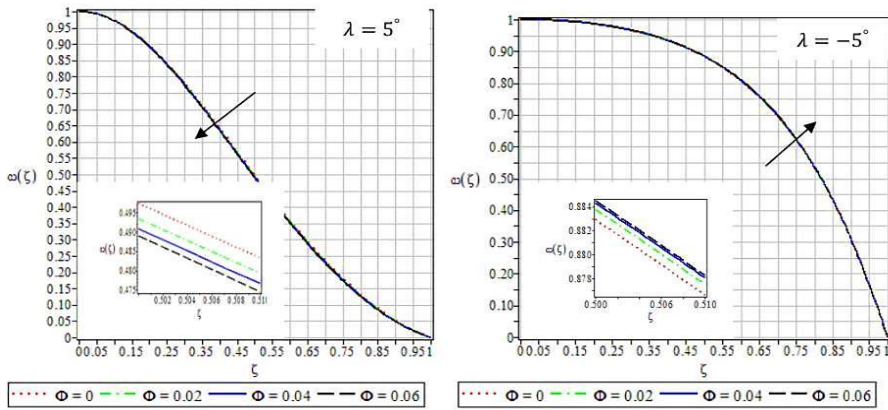
Figure 2. The behavior of the velocity  $\omega(\xi)$  for  $Al_2O_2$ .



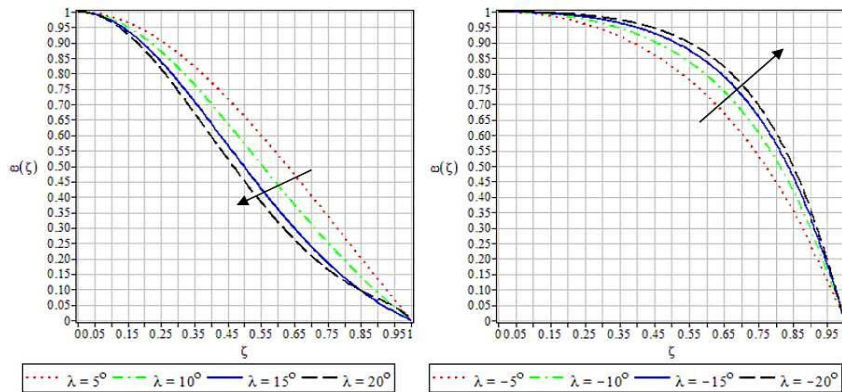
(a)  $\tilde{H}_a$  is varied for  $\tilde{R}_e = 100, \varphi = 0.05$



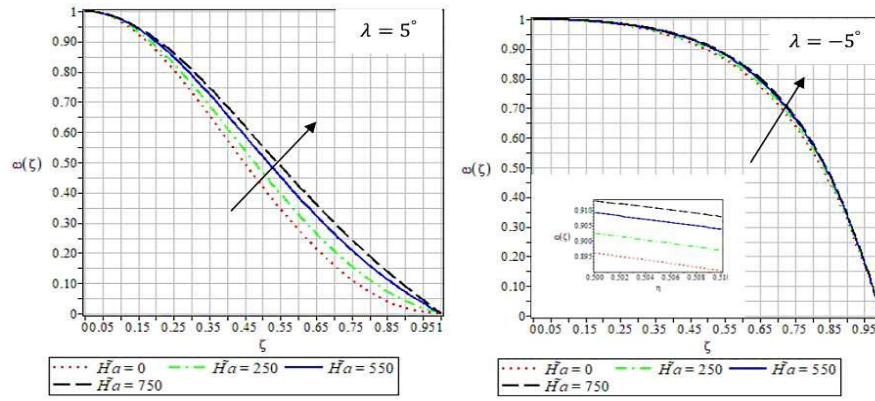
(b)  $\tilde{R}_e$  is varied for  $\tilde{H}_a = 50, \varphi = 0.05$



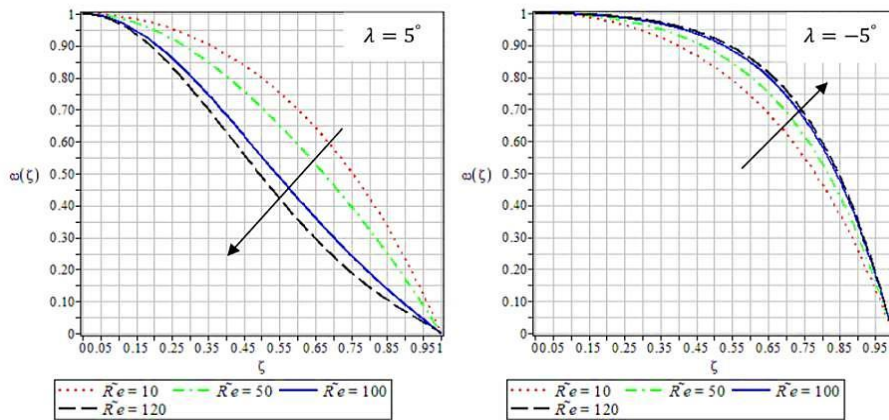
(c)  $\varphi$  is varied for  $\tilde{R}_e = 100, \tilde{H}_a = 50$



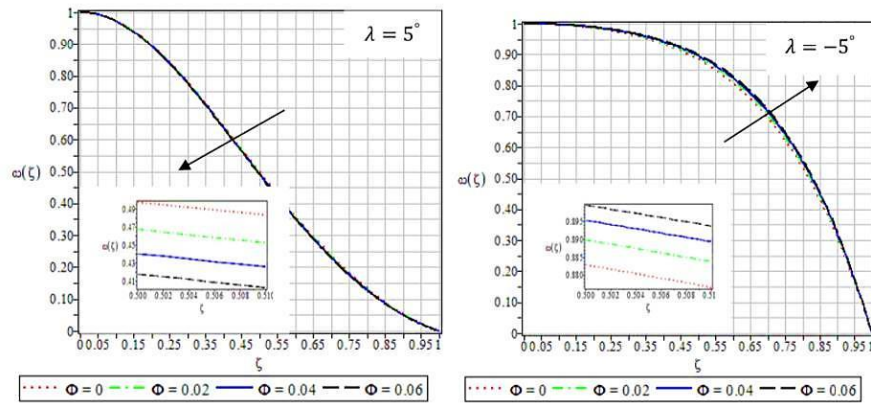
(d)  $\lambda$  is varied for  $\tilde{R}_e = 40, \tilde{H}_a = 50, \varphi = 0.05$   
Figure 3. The behavior of the velocity  $\omega(\xi)$  for  $\text{TiO}_2$ .



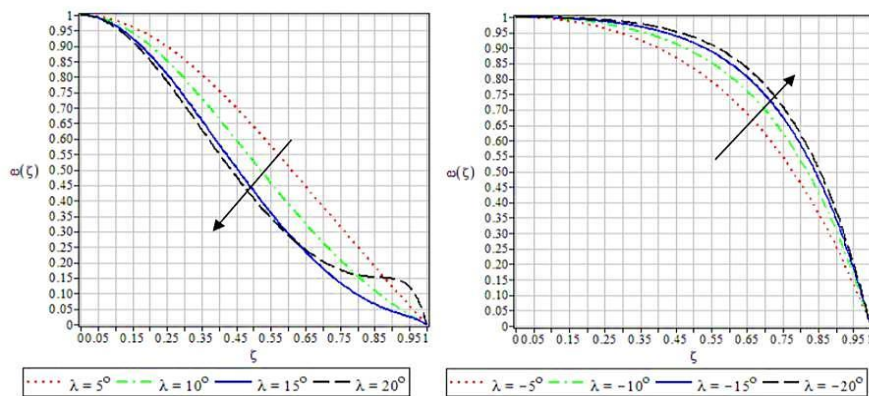
(a)  $\tilde{H}_a$  varied for  $\tilde{R}_e = 100, \varphi = 0.05$



(b)  $\tilde{R}_e$  varied for  $\tilde{H}_a = 50, \varphi = 0.05$



(c)  $\varphi$  varied for  $\tilde{R}_e = 100, \tilde{H}_a = 50$



(d)  $\lambda$  is varied for  $\tilde{R}_e = 40, \tilde{H}_a = 50, \varphi = 0.05$

Figure 4. The behavior of the velocity  $\omega(\xi)$  for Cu.

**The Criterion of Convergence**

In this section, the analysis of convergence<sup>24,25</sup> for approximate- analytical solutions obtained by applying the perturbation iteration scheme to Jeffery Hamel nanofluid flow is discussed.

From the theorems<sup>13</sup>, the convergence condition can be summarized as follows:

$$\beta_i = \begin{cases} \frac{\|C_{i+1}\|}{\|C_i\|}, & \|C_i\| \neq 0, \\ 0, & \|C_i\| = 0. \end{cases} \text{ For } i = 0,1,2, \dots$$

Then, we can say that the series approximate solutions  $\{\omega_n\}_0^\infty$  converges to the exact solution  $\omega$  which satisfy  $0 < \beta_i < 1$ . As a result, we will investigate the convergence of all the solutions from applying PIS with various parameters physical to the flow problem provided as in Tables 9-11:

**Table 9. The values of the convergence condition for  $\tilde{H}_a = 100, \varphi = 0.02$ .**

	Convergent Channel	Divergent Channel
$\tilde{R}_e = 10$	$\beta_0$ 0.1411810894	$\beta_0$ 0.07791235460
	$\beta_1$ 0.0935334332	$\beta_1$ 0.05724796917
	$\beta_2$ 0.0515927896	$\beta_2$ 0.03205946998
	$\vdots$	$\vdots$
	$\vdots$	$\vdots$
$\tilde{R}_e = 50$	$\beta_0$ 0.3863381649	$\beta_0$ 0.6896834846
	$\beta_1$ 0.3581219765	$\beta_1$ 0.4583435333
	$\beta_2$ 0.1968631136	$\beta_2$ 0.2943455867
	$\vdots$	$\vdots$
	$\vdots$	$\vdots$
$\tilde{R}_e = 70$	$\beta_0$ 0.4305492890	$\beta_0$ 0.9690339670
	$\beta_1$ 0.4851477564	$\beta_1$ 0.7640911730
	$\beta_2$ 0.2662747644	$\beta_2$ 0.5477475715
	$\vdots$	$\vdots$
	$\vdots$	$\vdots$

**Table 10. The values of the convergence condition for  $\tilde{R}_e = 60, \varphi = 0.05$ .**

	Convergent Channel	Divergent Channel
$\tilde{H}_a = 100$	$\beta_0$ 0.4135183495	$\beta_0$ 0.8735164047
	$\beta_1$ 0.4217938618	$\beta_1$ 0.5989330136
	$\beta_2$ 0.2316881525	$\beta_2$ 0.4047721428
	$\vdots$	$\vdots$
	$\vdots$	$\vdots$
$\tilde{H}_a = 500$	$\beta_0$ 0.4245427965	$\beta_0$ 0.6053471556
	$\beta_1$ 0.5145881398	$\beta_1$ 0.4478715869
	$\beta_2$ 0.2800577281	$\beta_2$ 0.2819873444
	$\vdots$	$\vdots$
	$\vdots$	$\vdots$
$\tilde{H}_a = 750$	$\beta_0$ 0.4228299262	$\beta_0$ 0.4512128494
	$\beta_1$ 0.5742276354	$\beta_1$ 0.3646051721
	$\beta_2$ 0.3112843779	$\beta_2$ 0.2190332775
	$\vdots$	$\vdots$
	$\vdots$	$\vdots$

**Table 11. The values of the convergence condition for  $\tilde{R}_e = 60, \tilde{H}_a = 1000$ .**

	Convergent Channel	Divergent Channel
$\varphi = 0.02$	$\beta_0$ 0.09226558641	$\beta_0$ 0.4642518368
	$\beta_1$ 0.1525787323	$\beta_1$ 0.3974196368
	$\beta_2$ 0.3430056094	$\beta_2$ 0.2387217804
	$\vdots$	$\vdots$
	$\vdots$	$\vdots$
$\varphi = 0.05$	$\beta_0$ 0.1205813049	$\beta_0$ 0.4378818589
	$\beta_1$ 0.2039766130	$\beta_1$ 0.3748808097
	$\beta_2$ 0.3623216572	$\beta_2$ 0.2233554244
	$\vdots$	$\vdots$
	$\vdots$	$\vdots$
$\varphi = 0.09$	$\beta_0$ 0.7017153800	$\beta_0$ 0.5816984975
	$\beta_1$ 0.4135136276	$\beta_1$ 0.4754310591
	$\beta_2$ 0.3797457088	$\beta_2$ 0.2967041282
	$\vdots$	$\vdots$
	$\vdots$	$\vdots$

From the above tables, it is noted that the value of  $\beta_i, i = 0,1,2, \dots$  are sandwiched between 0 and 1, therefore the presented solutions are convergence. Fig. 5 describes the curves behaviors of the fluid flow in convergent- divergent channels.

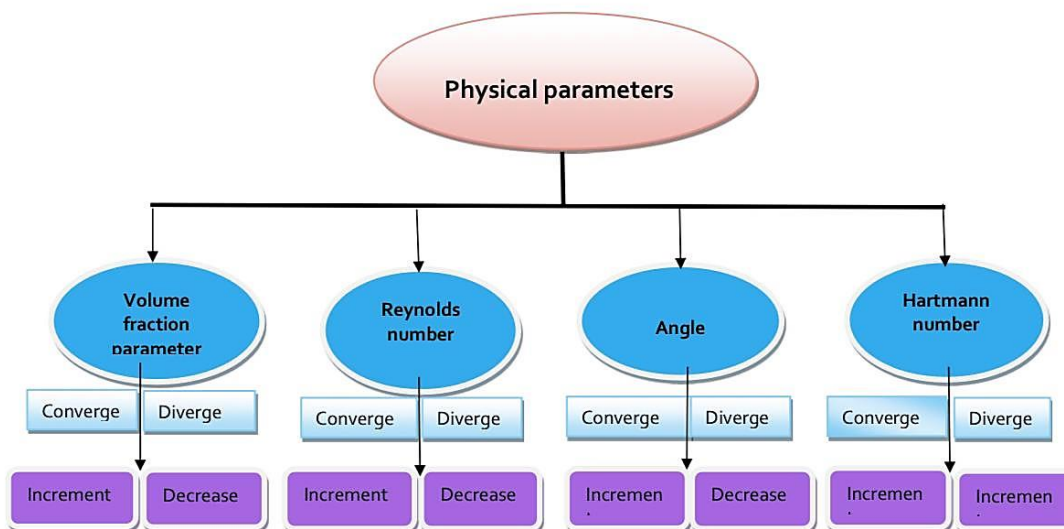


**Figure 5. The behaviors of the curves of velocity profiles.**

## Conclusion:

While working in this manuscript, the approximate analytical PIS of the velocity distribution of the Jeffrey-Hamel flow problem with nanoparticles was used. Since PIS is an effective and efficient approach to address all kinds of Jeffrey-Hamel flow problems, the method has been successfully demonstrated using similarity transformation through which the governing equations (continuity, momentum) of this problem have been converted into an ordinary differential equation, in addition to that it has been compared with other numerical methods. Note that the imposed method is more accurate among the methods, and the parameters were made semi-basically and their values were controlled to discuss the variation that occurs in the velocity profiles, as it was presented briefly in Fig. 5, which roughly illustrates the behavior that this method causes when changing the parameters on the velocity profile in the two converging/divergent channels. So, we can say that this method is useful to work on in detecting the behavior of nanofluids during their flow and knowing the velocity and convergence that they cause when taking water as a basic liquid with nanoparticles such as (copper, silver, titanium and aluminum). The future study of this method is done by expanding the horizons of working on nanofluids by taking fluids with higher densities. For example, we can replace water with oil or alcohol, or a mixture between oil and water, and so on, with different nanoparticles to obtain a more complex fluid and an advanced issue that can be used in various fields.

## Authors' Declaration:

- Conflicts of Interest: None.
- We hereby confirm that all the Figures and Tables in the manuscript are mine ours. Besides, the Figures and images, which are not mine ours, have been given the permission for re-publication attached with the manuscript.
- Ethical Clearance: The project was approved by the local ethical committee in University of Basrah.

## Authors' Contributions Statement:

A. M. conceived of the presented idea. S.I. performed the computations and verified the analytical method. All authors discussed the results and contributed to the final manuscript.

## References:

1. Kaggwa A., and Carson JK. Developments and future insights of using nanofluids for heat transfer enhancements in thermal systems: a review of recent literature. *Int Nano Lett* . 2019; 9(4): 277–288. <https://doi.org/10.1007/s40089-019-00281-x>.
2. Younes H., Mao M., Sohel Murshed SM., Lou D., Hong H., and Peterson GP. Nanofluids: Key parameters to enhance thermal conductivity and its Appl. Therm. Eng . 2022; Vol. 207: Elsevier Ltd. <https://doi.org/10.1016/j.applthermaleng.2022.118202>.
3. Jeffery GBL. The two-dimensional steady motion of a viscous fluid. *Lond. Edinb. Dublin philos. Mag. j. sci.*1915;29(172):455–465. <https://doi.org/10.1080/14786440408635327>.
4. Hamel G. Spiralförmige Bewegungen zäher Flüssigkeiten. *Jahresber Dtsch Math.-Ver*,1917; 25: 34-60. <http://eudml.org/doc/145468>.
5. Biswal U., and Chakraverty S. Investigation of Jeffery-Hamel Flow for Nanofluid in the Presence of Magnetic Field by a New Approach in the Optimal Homotopy Analysis Method. *JACM* . 2022; 8(1): 48–59. <https://doi.org/10.22055/jacm.2020.31909.1937>.
6. Singh J., Rashidi MM., Sushila, and Kumar DA. hybrid computational approach for Jeffery–Hamel flow in non-parallel walls. *Neural. Comput. Appl.* 2019; 31(7): 2407–2413. <https://doi.org/10.1007/s00521-017-3198-y>.
7. Chaharborj SS., and Moameni A. Spectral-homotopy analysis of MHD non-orthogonal stagnation point flow of a nanofluid. *J. Appl. Math. Comput. Mech.* 2018; 17(1): 15–28. <https://doi.org/10.17512/jamcm.2018.1.02>.
8. Petroudi IR., Ganji DD., Nejad MK., Rahimi J., Rahimi E., and Rahimifar A. Transverse magnetic field on Jeffery-Hamel problem with Cu-water nanofluid between two non-parallel plane walls by using collocation method. *Case Stud. Therm. Eng.* 2014; 4: 193–201. <https://doi.org/10.1016/j.csite.2014.10.002> .
9. Rahman I UR., Sulaiman M., Alarfaj FK., Kumam P., and Laouini G. Investigation of non-linear MHD Jeffery–Hamel blood flow model using a hybrid metaheuristic approach. *IEEE Access*. 2021;9: 163214–163232. <https://doi.org/10.1109/ACCESS.2021.3133815>.
10. Ahmad I., and Ilyas H. Homotopy Perturbation Method for the nonlinear MHD Jeffery–Hamel blood flows problem. *Appl. Numer. Math.* 2019; 141: 124–132. <https://doi.org/10.1016/j.apnum.2018.07.005>.
11. Li Z., Khan I., Shafee A., Tlili I., and Asifa T. Energy transfer of Jeffery–Hamel nanofluid flow between non-parallel walls using Maxwell–Garnetts (MG) and Brinkman models. *Energy Reports*. 2018; 4: 393–399. <https://doi.org/10.1016/j.egy.2018.05.003>.
12. Meher R., and Patel ND. Analytical Investigation of MHD Jeffery–Hamel flow problem with heat transfer by differential transform method. *SN Appl. Sci.* 2019; 1(7). <https://doi.org/10.1007/s42452-019-0632-z>.
13. Al-Saif, ASJ., and Harfash, AJ. Perturbation-iteration algorithm for solving heat and mass transfer in the unsteady squeezing flow between parallel plates. *J. Appl. Comput. Mech.* 2019; 5(4): 804–815. <https://doi.org/10.22055/JACM.2019.28052.1453>

14. Jasim A M. New Analytical Study for Nanofluid between Two Non-Parallel Plane Walls (Jeffery-Hamel Flow). J. Appl. Comput. Mech.. 2021; 7(1): 213–224. <https://doi.org/10.22055/jacm.2020.34958.2520>.
15. Jasim AM. New Analytical Study of Non-Newtonian Jeffery Hamel Flow of Casson Fluid in Divergent and Convergent Channels by Perturbation Iteration Algorithm. Baghdad J Sci. 2021; 39(1): 37–55. <https://doi.org/10.29072/basjs.202113>.
16. Kumbinaraiaiah S., and Raghunatha KR. Numerical solution of the Jeffery–Hamel flow through the wavelet technique. Heat Transfer. 2022; 51(2): 1568–1584. <https://doi.org/10.1002/htj.22364>.
17. Umavathi J C., and Shekar M (n.d.). Effect of MHD on Jeffery-Hamel Flow in Nanofluids by Differential Transform Method. J. Eng. Res. Appl. . 2022 ;(Vol. 3). [www.ijera.com](http://www.ijera.com).
18. Mehmood A., Ul-Haq N., Zameer A., Ling SH., Asif M., and Raja Z (n.d.). Design of Neuro-Computing Paradigms for Nonlinear Nanofluidic Systems of MHD Jeffery-Hamel Flow. J. Taiwan Inst. Chem. 2018;Vol.(91):57-85. <https://www.sciencedirect.com/science/article/pii/S1876107018303201>.
19. AL-Jizani, K H., and Al-Delfi J KK. An Analytic Solution for Riccati Matrix Delay Differential Equation using Coupled Homotopy-Adomian Approach. Baghdad Sci J. 2022; 19(4): 800–804. <https://doi.org/10.21123/bsj.2022.19.4.0800>.
20. Al-Jawary MA, and Salih OM. Effective Computational Methods for Solving the Jeffery-Hamel Flow Problem. Baghdad Sci J. 2022. <https://doi.org/10.21123/bsj.2022.7326>.
21. Noon, N J. Numerical Analysis of Least-Squares Group Finite Element Method for Coupled Burgers' Problem. Baghdad Sci J.2022; 18(4): 1521–1535. [https://doi.org/10.21123/bsj.2021.18.4\(Suppl.\).1521](https://doi.org/10.21123/bsj.2021.18.4(Suppl.).1521).
22. Swaidan W., and Ali H S. Numerical solution for linear state space systems using haar wavelets method. Baghdad Sci J. 2022; 19(1): 84–90. <https://doi.org/10.21123/BSJ.2022.19.1.0084>.
23. Tarrad AH. 3D Numerical Modeling to Evaluate the Thermal Performance of Single and Double U-tube Ground-coupled Heat Pump. High Tech Innov. J. 2022; 3(2): 115–129. <https://doi.org/10.28991/HIJ-2022-03-02-01>.
24. Hasan P M., and Sulaiman N A. Convergence Analysis for the Homotopy Perturbation Method for a Linear System of Mixed Volterra-Fredholm Integral Equations. Baghdad Sci J. 2020; 17(3(Suppl.)): 1010. [https://doi.org/10.21123/bsj.2020.17.3\(Suppl.\).1010](https://doi.org/10.21123/bsj.2020.17.3(Suppl.).1010).
25. Hasim I, Kilicman A, Ismail AI, Azmi A, and Che Hussin CH. Approximate Analytical Solutions of Bright Optical Soliton for Nonlinear Schrödinger Equation of Power Law Nonlinearity. Baghdad Sci J.2021; 18(1(Suppl.)). [https://doi.org/10.21123/bsj2021.18.1\(Suppl.\).0836](https://doi.org/10.21123/bsj2021.18.1(Suppl.).0836).

## التقييم شبه التحليلي لتدفق السائل النانوي المغنطيسي الهيدروديناميكي مشكلة جيفري هامل

عبيد مجيد جاسم

سجى عصام عبد الرضا

قسم الرياضيات، كلية العلوم، جامعة البصرة، البصرة، العراق.

### الخلاصة:

في هذا البحث تمت دراسة تحليل مشكلة المغنيسيوم والديناميكا المائية غير البعدية باستخدام الجسيمات النانوية في تدفق جيفري هامل (JHF). يتم تقليل المعادلات الأساسية لهذه المسألة إلى معادلة تفاضلية اعتيادية من ثلاثة مستويات. يدرس المشروع الحالي تأثير الزوايا بين الصفائح، ورقم رينولدز، ومعلمة حجم الجسيمات النانوية، والرقم المغنطيسي على توزيع السرعة باستخدام تقنية تحليلية تعرف بمخطط الاضطراب التكراري (PIS). يتشابه تأثير هذه المعلمات في القنوات المتقاربة والمتباعدة باستثناء الرقم المغنطيسي الذي يختلف في القناة المتباعدة. علاوة على ذلك، فإن الحلول الناتجة ذات التقارب الجيد والدقة العالية للقيم المختلفة للمعلمات الفيزيائية هي في شكل سلسلة طاقة للمشكلة المطروحة. تظهر كفاءة هذه الطريقة من خلال المقارنة بين الحالات المختلفة بين النتائج المحسوبة مع الحل العددي والحلول بطرق أخرى.

**الكلمات المفتاحية:** تحليل التقارب، الديناميكا المائية المغنطيسية، تدفق السوائل النانوية، الصفائح غير المتوازية، الجسيمات النانوية.